
Global Patterns of Nonlinearity in Real and GCM-Simulated Atmospheric Data

Jiří Mikšovský, Petr Pišoft, and Aleš Raidl

Department of Meteorology and Environment Protection, Faculty of Mathematics and Physics, Charles University, Prague, Czech Republic,
jiri.miksovsky@mff.cuni.cz; petr.pisoft@mff.cuni.cz;
ales.raidl@mff.cuni.cz

Abstract. We employed selected methods of time series analysis to investigate the spatial and seasonal variations of nonlinearity in the NCEP/NCAR reanalysis data and in the outputs of the global climate model HadCM3 of the Hadley Center. The applied nonlinearity detection techniques were based on a direct comparison of the results of prediction by multiple linear regression and by the method of local linear models, complemented by tests using surrogate data. Series of daily values of relative topography and geopotential height were analyzed. Although some differences of the detected patterns of nonlinearity were found, their basic features seem to be identical for both the reanalysis and the model outputs. Most prominently, the distinct contrast between weak nonlinearity in the equatorial area and stronger nonlinearity in higher latitudes was well reproduced by the HadCM3 model. Nonlinearity tends to be slightly stronger in the model outputs than in the reanalysis data. Nonlinear behavior was generally stronger in the colder part of the year in the mid-latitudes of both hemispheres, for both analyzed datasets.

Keywords: Nonlinearity, Reanalysis, Global climate model, Surrogates

1 Introduction

The Earth's climate system, as well as its atmospheric component, is an intrinsically nonlinear physical system. This nonlinearity is generally reflected in many series of climatic variables such as atmospheric pressure or temperature, but whether it is detectable and how strong it is depends on the type of the variable [1, 2, 3], geographic area of its origin [2, 4, 5, 6] or length of the signal [3]. The manifestations of nonlinearity in time series can be studied in numerous ways, using different statistics or criteria of the presence of nonlinear behavior. The techniques applied so far to meteorological data involve the calculation of the mutual information or persistence [1, 7, 8], statistics based on the performance of a nonlinear predictive method [3, 4, 9], nonlinear correlations [10] or the examination of the character of the prediction

residuals [2, 4, 5]. Tests using some form of surrogate data are frequently employed [1, 2, 3, 4, 7, 9, 10]. The presence of nonlinearity can also be assessed by comparing the performance of a linear and a nonlinear time series analysis method. In the atmospheric sciences, such studies are frequently associated with the application of statistical methods for prediction [6, 11, 12], or downscaling and postprocessing tasks [6, 13, 14, 15, 16]. Alongside with a wide spectrum of techniques for the detection of nonlinearity, different authors studied diverse types of signals, ranging from various variables related to the local temperature [1, 3, 6, 7, 10, 13, 14, 15, 16] or pressure [1, 2, 3, 4, 5, 7] to characteristics of larger-scale dynamics such as the mean hemispheric available potential energy [8]. Heterogeneity of the methods and datasets applied by different researchers makes it difficult to directly compare the results and use them to create a consistent global picture of the geographic variations of nonlinearity. However, it also seems that there are some systematic regularities in the spatial distribution of nonlinearity or of the related characteristics [2, 5, 6, 10, 17]. Here, we investigate this matter further, using a comparison of the results of linear and nonlinear prediction and tests based on the surrogate data.

A significant portion of the existing studies dealing with the issue of nonlinearity in time series focus on the analysis of individual scalar signals, typically employing time delayed values for the construction of the space of predictors or phase space reconstruction. Due to the complex behavior the atmosphere exhibits, and the relatively small size of the available records, the information content in a single series is limited and often insufficient for an effective application of nonlinear techniques. But meteorological measurements are frequently available for more than one variable, and they are carried out at multiple locations. When a multivariate system is used instead of a single scalar series, more information about the local state of the climate system can be obtained. It also seems that multivariate systems exhibit a generally stronger detectable nonlinear behavior [3]. For these reasons, and because using multiple input variables is common in many tasks of statistical meteorology and climatology, we focused on settings with multivariate predictors in this study. We restricted our attention to just a few of the available variables, defining the temperature and pressure structure of the atmosphere. The two illustrative cases presented here are based on forecasts of daily values of the relative topography 850-500 hPa (which is closely related to the temperature of the lower troposphere) and of the geopotential height of the 850 hPa level (one of the variables characterizing the structure of the field of atmospheric pressure). Along with investigating the character of the series derived from actual measurements (NCEP/NCAR reanalysis), attention was paid to the potential of the global climate model HadCM3 to reproduce the structures detected in the observed data. This should help to assess whether such simulation is able to capture not just the basic characteristics of the Earth's climate, but also the eventual nonlinear features of the respective time series. The utilized datasets are presented in Sect. 2, the techniques applied to quantitatively evaluate

nonlinearity are described in Sect. 3. Section 4 is devoted to the study of the spatial variations of nonlinearity. Section 5 focusses on the influence of the presence of the annual cycle in the series and seasonal changes of the detected patterns. Finally, in Sect. 6, the results are discussed with regard to their possible physical cause and practical implications. Color versions of the presented maps of the geographical distribution of nonlinearity (Figs. 3, 5, 6, 8 and 9) can be accessed at <http://www.miksovsky.info/springer2008.htm>.

2 Data

Direct atmospheric observations and measurements suffer from a number of potential problems. Their locations are typically unevenly spaced and coverage of some areas of the Earth is limited. Data from different sources are often incompatible and sometimes flawed. This restricts the usability of raw measurements for an analysis such as ours, the goal of which is to derive globally comparable results. To avoid or reduce the aforementioned problems, we used a gridded dataset in this study instead of direct measurements – the NCEP/NCAR reanalysis [18, 19] (hereinafter NCEP/NCAR). The reanalysis is a dataset derived from measurements at weather stations, as well as inputs from rawinsondes, meteorological satellites and other sources. The input observations are processed by a fixed data assimilation system, including a numerical forecast model, and the resulting series are available in a regular horizontal grid of 2.5° by 2.5° . Here, daily values of the geopotential height of the 850 hPa level (hereinafter H850) and 500 hPa level have been employed in a reduced 5° by 5° horizontal resolution, for the period between 1961 and 2000. From the values of the geopotential heights, the relative topography 850-500 hPa (RT850-500) has been computed. This quantity describes the thickness of the layer between the 850 hPa and 500 hPa levels and it is proportional to its mean virtual temperature. According to the classification used by Kalnay et al. [18], geopotential heights fall into the A-category of variables, thus reflecting the character of actual measurements rather than the specific properties of the model applied to create the reanalysis. A typical example of the analyzed series of RT850-500 in the equatorial area and in the mid-latitudes is shown in Fig. 1.

The recently increased interest in climate change instigated an intensive development of the models of the global climate. These simulations, to be reasonably realistic, must describe all key components of the climate system as well as the connections among them. As a result, the models are very complex and demanding with respect to the required computational resources. But despite their sophistication, no model is able to mimic the observed climate with absolute accuracy. A very important task in climate modeling is therefore validating the models, i.e., assessing their ability to reproduce the real climate. The common validation procedures are usually based on the basic statistical characteristics of the model outputs; here, we focus on the ability of a climate

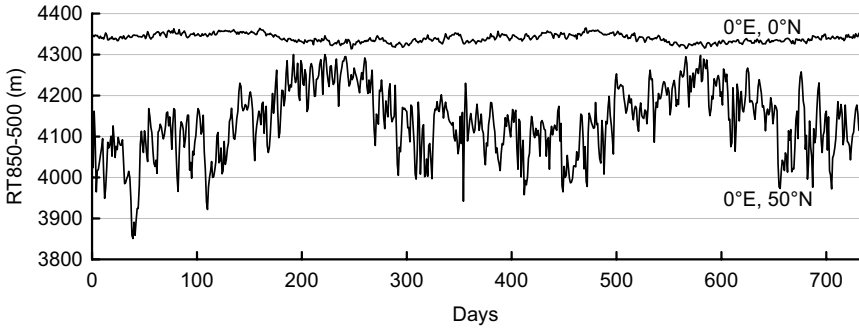


Fig. 1: A section of the analyzed data: Time series of daily values of the relative topography 850-500 hPa in the equatorial area (0°E , 0°N) and in the mid-latitudes (0°E , 50°N), for the years 1991 and 1992.

simulation to produce time series with the same nonlinear qualities as the real climate. For this task, we chose one of the major global climate models, HadCM3 of the Hadley Centre [20, 21]. The model outputs were used in a reduced horizontal resolution of 3.75° (longitude) by 5° (latitude). The model integration employed here was based on the observed concentrations of the greenhouse gasses and estimates of past changes in ozone concentration and sulfur emissions prior to the year 1990, and the emission scenario SRES B2 afterwards [21]. Since we only used the period from 1961 to 2000 for our analysis, and there is just very little difference among the SRES scenarios in the 1990s, the specific scenario choice should not be crucial.

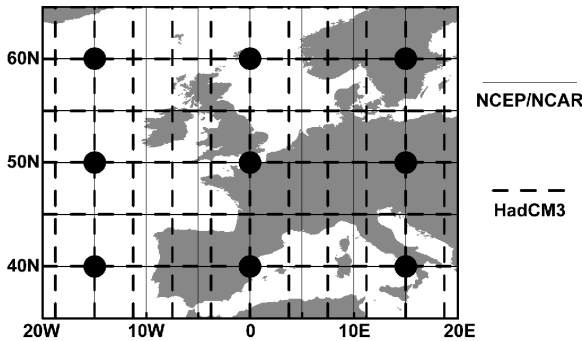


Fig. 2: An example of the structure of the pattern of predictors, displayed for the predictand series located at 0°E , 50°N . Black circles mark the positions of the predictors, the grid illustrates the reduced horizontal resolution of the NCEP/NCAR and HadCM3 data, used in this study.

3 Methods

3.1 General Settings

One of the key issues of the multivariate approach to the construction of the space of predictors is the selection of a suitable set of input variables. Unlike for some simple low-dimensional dynamical systems, a perfect phase-space reconstruction is impossible from climatic time series, due to the complexity of the underlying system. In the case of practical time series analysis tasks, a finite-dimensional local approximation of the phase space may suffice. To predict values of a scalar series in some grid point, we used a pre-set pattern of predictors, centered on the location of the predictand and spanning 30° in longitude and 20° in latitude (Fig. 2). A different configuration of predictors was chosen for each of the two tasks presented: In the case of the RT850-500 forecast, the dimension of the predictor space was $N = 18$, with 9 values of RT850-500 and 9 values of H850 in a configuration shown in Fig. 2. For the forecast of H850, 9 predictors were used, all of which were of the H850 type. Note that, despite the different spatial resolution of the NCEP/NCAR reanalysis and the HadCM3 model, the selected pattern of predictors could be applied for both of them directly, without interpolating the data to a common grid.

All predictors $x_i(t), i = 1, \dots, N$, were transformed to have zero mean and standard deviation equal to $\sqrt{\cos\varphi}$, using the linear transformation $x_i(t) \rightarrow \sqrt{\cos(\varphi)}(x_i(t) - \bar{x}_i)/\sigma_i$ (φ being latitude of the respective grid point, \bar{x}_i mean value of the predictor series and σ_i its standard deviation). Hence, the predictor's variance was proportional to the size of the area characterized by the corresponding grid point. The presented results were derived from the outcomes of prediction one day ahead, carried out for grid points located between 70°N and 70°S (the areas closest to the poles were excluded from the analysis, due to the severe deformation of the applied spatial pattern of predictors in high latitudes).

3.2 Direct Comparison-Based Approach

Our primary technique of quantification of nonlinearity was based on a direct comparison of the root mean square errors (RMSEs) of prediction by a linear reference method, multiple linear regression, and by its nonlinear counterpart, the method of local linear models. In the case of linear regression, the value of the scalar predictand y at time $t + 1$ was computed as a linear combination of the values of individual predictors $x_i, i = 1, \dots, N$, in the previous time step

$$\hat{y}(t + 1) = a_0 + \sum_{i=1}^N a_i x_i(t), \quad (1)$$

where the coefficients $a_j, j = 0, \dots, N$, were calculated to minimize the sum of the squared values of the residuals $\hat{y}(t) - y(t)$.

Even a nonlinear system can be described rather well when the linear model is applied locally for smaller portions of the phase space instead of a global linear approximation. This concept has been successfully utilized for the construction of forecast models for many different types of time series. Several related studies are reprinted in [22] and the basic principles of the method of local models are also described, e.g., in [23]. The dynamics in the individual regions of the input space is approximated by linear mappings based on (1), but an individual linear predictive model (or a set of coefficients a_i , respectively) is constructed for each value of t . To create such a local model, only a certain number M of the predictors-predictand pairs, representing the states of the system most similar to the one at time t , is employed to compute the coefficients. The similarity of individual states was quantified by the distance of the respective N -dimensional vectors of predictors $\mathbf{x}(t) = (x_1(t), x_2(t), \dots, x_N(t))$ here, using the Euclidian norm.

To calculate the out-of-sample root mean square error of the prediction, the analyzed series were divided into two subintervals. The years 1961–1990 were used as a calibration set, i.e., for the computation of the coefficients of the above described models. These were then tested for the years 1991–2000. The values of RMSE we obtained for the prediction by multiple linear regression ($RMSE_{\text{MLR}}$) and local linear models ($RMSE_{\text{LM}}$) were compared by computing

$$SS_{\text{LM}} = 1 - (RMSE_{\text{LM}}/RMSE_{\text{MLR}})^2, \quad (2)$$

which will be referred to as the local models' skill score. Its definition is based on the commonly used concept of a skill score, described, e.g., in [24]. SS_{LM} vanishes when both methods perform equally well in terms of RMSE and it equals to one for a perfect forecast by local models (presuming that $RMSE_{\text{MLR}} \neq 0$). The number M of predictors-predictand pairs used for the computation of the coefficients of the local models is one of the adjustable parameters of the method of local models. Depending on the specific structure of the local climate system, different values of M may be suitable to minimize RMSE. Here, local models constructed with $M = 250, 500$ and 1000 were tested for each grid point; the variant giving the lowest RMSE was then used in the subsequent analysis.

3.3 Surrogate Data-Based Approach

The above described approach yields results which are interesting from a practical perspective, but, strictly speaking, it only refers to a relation of two particular techniques, both of which may have their specifics. Another method, which does not rely on comparing different mappings, exists. It uses modified series (so-called surrogate series or surrogates), which preserve selected properties of the original signal, but are consistent with some general null hypothesis. Here, the hypothesis is that the data originates from a linear

Gaussian process, the output of which may have been modified by a static monotonic nonlinear filter. The values of a nonlinearity-sensitive statistic are then compared for the original series and multiple surrogates, and if a statistically significant difference is detected, the null hypothesis is rejected. It should be noted that the formal rejection does not necessarily prove the presence of nonlinearity in the signal, as it can be caused by other reasons, such as nonstationarity of the series or imperfection of the surrogate-generating procedure. For details see, e.g., [9], where the principles of the surrogate data-based tests are presented in depth, or [25], where the usability of several methods of generating surrogates is discussed for various geophysical data.

For each grid point, 10 surrogates were created from the respective multivariate system of time series. Prediction by the method of local linear models was carried out for each of the surrogates and an arithmetic average $RMSE_{\text{Surr}}$ of the resulting RMSEs was computed. A skill score-based variable, analogous to (2), was then calculated using RMSE for the original series $RMSE_{\text{LM}}$ and $RMSE_{\text{Surr}}$:

$$SS_{\text{Surr}} = 1 - (RMSE_{\text{LM}}/RMSE_{\text{Surr}})^2. \quad (3)$$

In order to keep the computational demands at a reasonable level, the surrogate data-based analysis was performed just for $M = 250$. Also, the years 1991–2000 were used for both calibration and testing of the mappings. The surrogate series were generated by the iterative amplitude adjusted Fourier transform [26] in its multivariate form [9]; the program package TISEAN by Hegger et al. [27] was applied for this task.

4 Spatial Patterns of Nonlinearity

Figure 3a shows the geographical distribution of the local models' skill score SS_{LM} , obtained for the NCEP/NCAR RT850-500 forecast. The most prominent feature of the detected pattern is the strong latitudinal variance of nonlinearity. Near the equator, just very small and mostly statistically insignificant difference between the performance of purely linear regression and local linear models was found. Nonlinear behavior becomes visibly stronger in the mid-latitudes, and it is more pronounced on average in the northern hemisphere, where major nonlinearity was detected for all grid points north of circa 25°N (Fig. 4). In the southern hemisphere, the strongest nonlinearity was located in a band approximately between 25°S and 50°S . This structure seems to be well reproduced by the HadCM3 model (Fig. 3b), although the nonlinear behavior is slightly stronger in the model data in the northern hemisphere – see Table 1, columns 1 and 2. The spatial correlation of the SS_{LM} fields for the NCEP/NCAR and HadCM3 data was evaluated by computing the Pearson correlation coefficient, after linear interpolation of the HadCM3 data-based values of SS_{LM} to the 5° by 5° grid of NCEP/NCAR. For the entire area

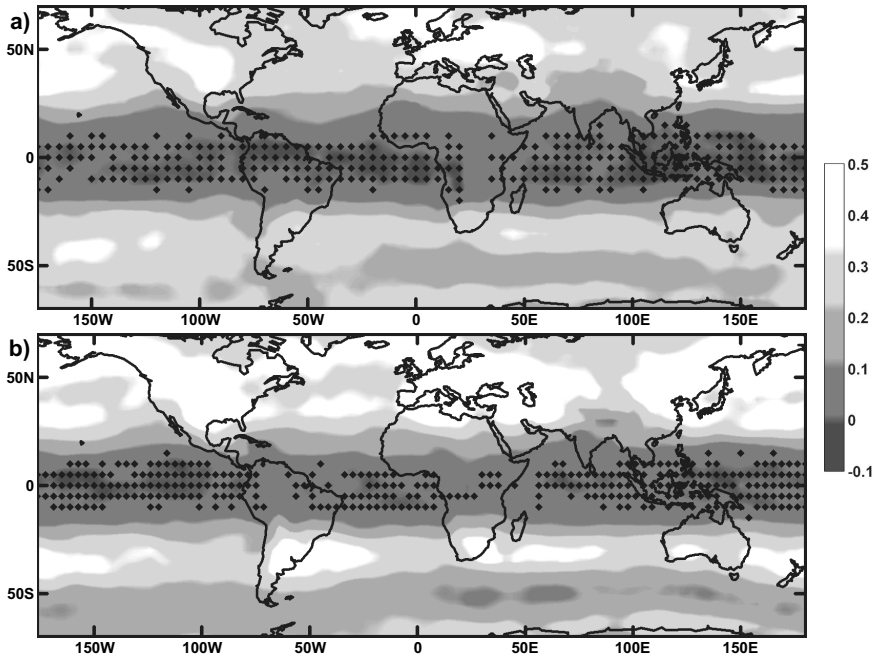


Fig. 3: Geographical distribution of the local models' skill score SS_{LM} , obtained for the RT850-500 prediction, using the NCEP/NCAR (a) and HadCM3 (b) data. Diamonds mark the positions of the grid points where daily errors of prediction by the method of local models were not statistically significantly lower than for linear regression at the 95% confidence level, according to the one-sided paired sign test.

between 70°N and 70°S , the correlation was 0.91. When just extratropical areas were taken into account, the resemblance of the SS_{LM} patterns was stronger in the northern hemisphere than in the southern one (Table 1, column 3). Similar values of correlation were also obtained when the Spearman rank-order correlation coefficient was used instead of the Pearson one.

Aside from the dominant latitudinal dependence, the detected nonlinearity patterns also exhibited a distinct finer structure. As can be seen in Fig. 3a for the NCEP/NCAR reanalysis data, local maxima of nonlinearity were found over Europe, North America, East Asia and the northern part of the Pacific Ocean, and east of the landmasses of the southern hemisphere. The HadCM3 data yielded a very similar pattern (Fig. 3b). After the average latitudinal structure was filtered out by subtracting the respective latitudinal averages from the values of SS_{LM} in every grid point, the spatial correlation of the NCEP/NCAR and HadCM3 SS_{LM} patterns was still rather high, though the resemblance of both fields was clearly stronger in the northern hemisphere (Table 1, column 4).

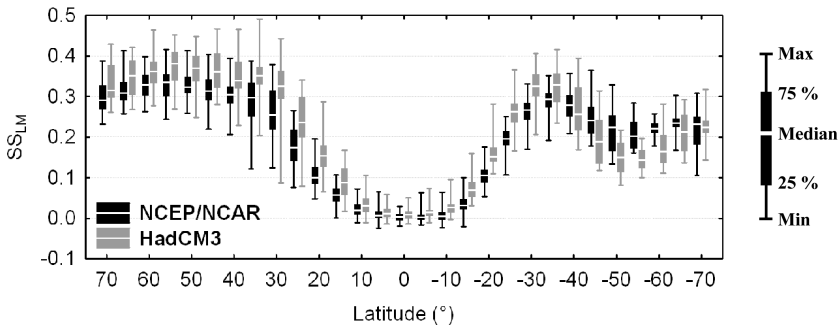


Fig. 4: Distribution of SS_{LM} in different latitudes, obtained for the RT850-500 prediction (latitude values are positive north of the equator).

Table 1: Regional averages of SS_{LM} , obtained for the RT850-500 prediction in the case of the NCEP/NCAR (column 1) and HadCM3 (column 2) data and spatial correlations of the NCEP/NCAR and HadCM3 SS_{LM} patterns for the original values of SS_{LM} (column 3) and after the average latitudinal dependence has been filtered out (column 4).

Region	SS_{LM}		Correlation	
	NCEP/NCAR	HadCM3	Original	Filtered
25°N–70°N	0.29	0.34	0.75	0.60
20°S–20°N	0.04	0.06	0.89	0.45
70°S–25°S	0.24	0.23	0.55	0.48

When the results of the H850 prediction were applied as a basis for a nonlinearity detection, a somewhat different pattern emerged (Fig. 5). The basic latitudinal structure with very weak nonlinearity in the equatorial area was still present, but other details of the detected structure differed from the ones found for the RT850-500 prediction. In the northern hemisphere, maximum values of SS_{LM} were located over the northwestern part of the Atlantic Ocean and the adjacent part of North America, as well as over the northern part of the Pacific Ocean. Both these maxima were rather well expressed, while the rest of the northern hemisphere exhibited weaker nonlinearity. In the southern hemisphere, the maxima of SS_{LM} were less localized. The overall degree of nonlinearity was lower than for the RT850-500 prediction (Table 2, columns 1 and 2). The similarity of the patterns obtained from the NCEP/NCAR and HadCM3 data was again very strong, with a value of global spatial correlation of 0.9. The nonlinearity was stronger on average in the HadCM3 outputs than in the NCEP/NCAR reanalysis. As for the match of the patterns of SS_{LM} with filtered-out latitudinal dependence, there was still a high positive correlation, stronger in the northern hemisphere (Table 2, column 4).

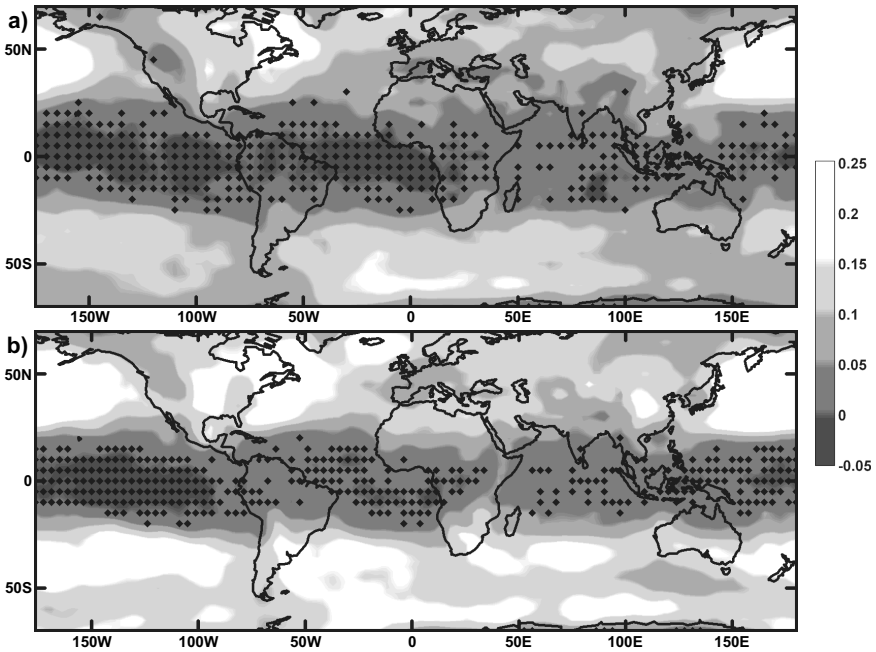


Fig. 5: Same as Fig. 3, for the prediction of H850 instead of RT850-500.

Table 2: Same as Table 1, for the prediction of H850 instead of RT850-500.

Region	SS_{LM}		Correlation	
	NCEP/NCAR	HadCM3	Original	Filtered
25°N–70°N	0.10	0.13	0.84	0.85
20°S–20°N	0.02	0.03	0.71	0.52
70°S–25°S	0.09	0.14	0.75	0.71

As can be seen from Fig. 6, the pattern of nonlinearity obtained for the RT850-500 prediction by means of surrogate data and expressed through SS_{Surr} is very similar to the one presented above for the direct comparison technique (Fig. 3a). To illustrate the distribution of RMSE in the ensemble of surrogates, a more detailed example of the outcomes is shown in Fig. 7 for the grid points along the 0° meridian. The results for the HadCM3 data are not shown, but they also confirm the outcomes of the direct comparison of multiple linear regression and local linear models. Similarly, surrogate data-based verification of the results derived from the H850 prediction showed no major differences either.

It should be mentioned that when an identical setting is used for direct comparison-based and surrogate data-based tests, including an equal size of the calibration set, SS_{LM} is systematically smaller than SS_{Surr} . The reason

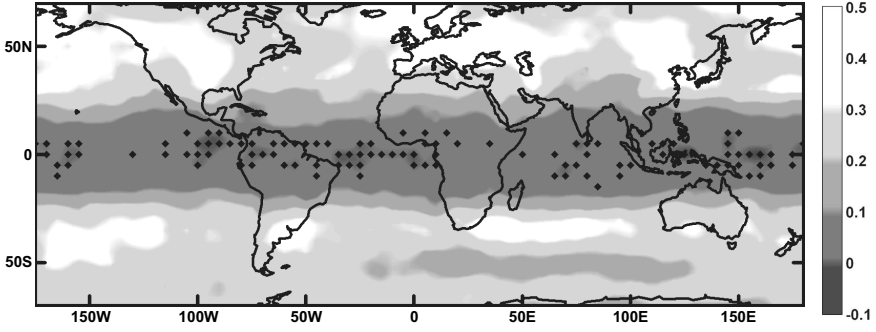


Fig. 6: Geographical distribution of SS_{SURR} , obtained for the RT850-500 prediction, using the NCEP/NCAR data. Diamonds mark positions of the grid points, where the value of RMSE for the original series was not smaller than for all 10 surrogates. This is equivalent to the non-rejection of the hypothesis of a linear Gaussian generating process at the confidence level of about 91%, according to the usually applied one-sided rank-order test, described, e.g., in [9]. Testing at a higher confidence level would require more surrogates, but even then, the results would be almost identical, as additional tests have shown for selected individual grid points.

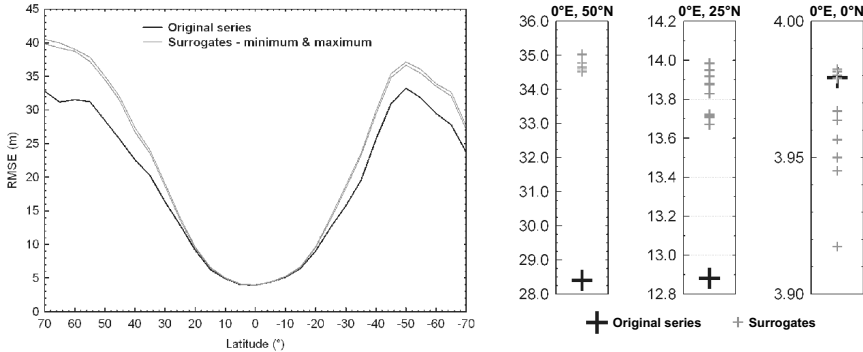


Fig. 7: *Left panel*: RMSE of the RT850-500 prediction by the local linear models method and its range for the respective surrogate series, for grid points at 0°E (NCEP/NCAR data). *Right panels*: Values of RMSE (m) obtained for the original series and individual surrogates in the three selected grid points.

for this difference is related to the behavior of the method of local models for purely linear series. When the processed signal contains no deterministic nonlinear component (like surrogates do) and M is smaller than the size of the calibration set, the method of local models performs slightly worse than linear regression. Our choice of a shorter calibration set for the surrogate data-based tests (Sect. 3.3) has actually partly compensated for this shift, because the magnitude of detected nonlinearity generally decreases with the reduction of the size of the calibration set.

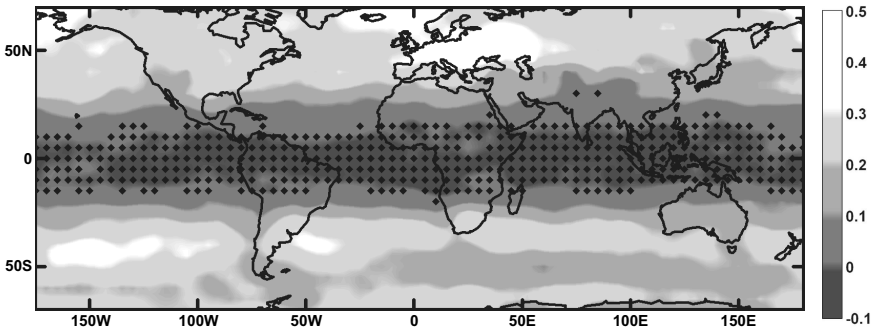


Fig. 8: Same as Fig. 3a, for series with removed annual cycle.

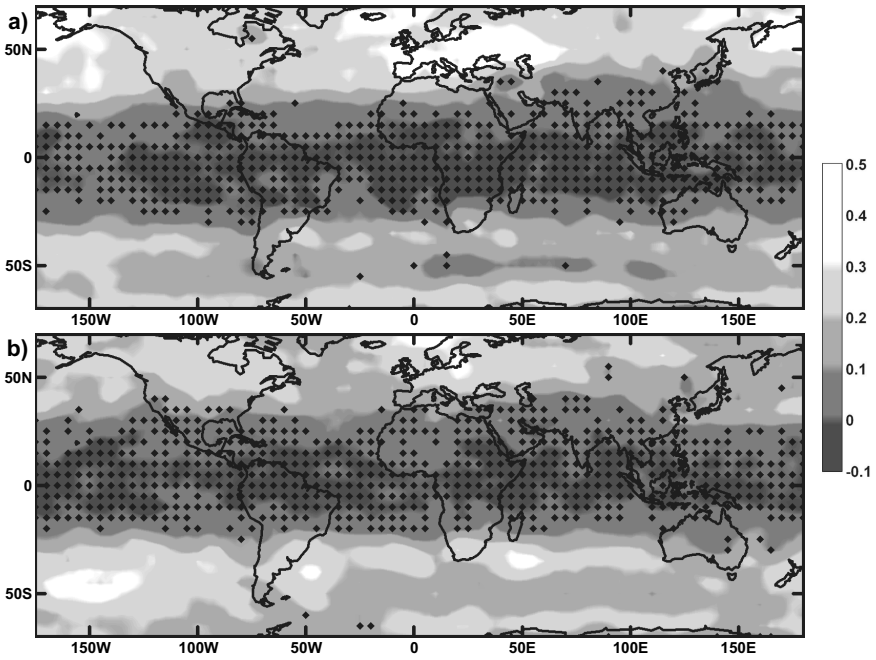


Fig. 9: Same as Fig. 3a, for the DJF (a) and JJA (b) seasons (winter and summer in the northern hemisphere) instead of the entire year.

5 Seasonal Variations of Nonlinearity

The annual cycle is among the strongest oscillations in the climate system. It dominates series of many climatic variables, especially in higher latitudes (see example in Fig. 1). This also means that the geographical areas with a well-defined annual cycle coincide to some degree with the regions, where strong nonlinearity was detected. To assess the possible relationship, we repeated some of the tests for the series with removed annual cycle. The removal was carried out by subtracting the mean climatological annual cycle of the respective variable, computed for the years 1961–2000 and smoothed by an 11-day moving average. An example of the results is shown in Fig. 8, for the RT850-500 prediction. As a comparison to Fig. 3a reveals, the values of SS_{LM} generally decreased after the annual cycle removal. Although this change was relatively small on average (e.g., the average value of SS_{LM} decreased from 0.29 to 0.23 in the area north of 25°N, and from 0.24 to 0.21 south of 25°S), it was profound in the regions with the highest amplitude of the annual cycle of RT850-500. For instance, the maximum of SS_{LM} , originally detected over East Asia and the adjacent part of the Pacific Ocean, disappeared almost completely. In the southern hemisphere, the changes associated with the annual cycle removal were generally smaller. In the case of the H850 prediction, the shape of the pattern of SS_{LM} remained practically identical for the annual cycle-free series, though the average degree of nonlinearity also slightly decreased.

In many situations, the annual cycle cannot be treated as simply an oscillation superposed to the variations at other time scales. Different seasons are associated with different atmospheric dynamics in many regions, and properties of the analyzed time series, including their eventual nonlinearity, may thus periodically vary throughout the year. Because of this, the analysis of climatic data is often performed separately for different parts of the year, typically seasons or months. We used this approach to investigate the seasonal variations of SS_{LM} . The results below are shown for the parts of the year corresponding to climatological winter (December, January and February – DJF) and summer (June, July and August – JJA) of the northern hemisphere. When the analysis was carried out for separate seasons, the RMSE of the prediction by linear regression decreased for most grid points in the annual average. The performance of the method of local models usually became worse, primarily due to the reduction of the amount of data available for the calibration of the mappings. As a result, the average magnitude of nonlinearity decreased somewhat, compared to the situation when the series were analyzed as the whole. Despite this change, the basic features of the patterns of SS_{LM} were still the same, as can be seen from an example of the results based on the RT850-500 forecast (Fig. 9). In the equatorial area, the nonlinearity remained very weak or undetectable in all seasons. In higher latitudes, the patterns retained some of the basic shape, detected for the year as the whole, but their magnitude visibly varied with the season. The overall nonlinearity was stronger in the

DJF season than in JJA in the northern hemisphere, while in higher latitudes of the southern hemisphere, this variation was reversed and JJA exhibited stronger nonlinearity than DJF on average (Fig. 10, Table 3, columns 1 and 2). The seasonal changes were stronger expressed in the northern hemisphere. The seasonal variation was well simulated by the HadCM3 model (Table 3, columns 3 and 4) and it was also detectable in the results based on the forecast of H850, for both the NCEP/NCAR and HadCM3 data (not shown).

6 Discussion

All performed analyses revealed a common basic latitudinal structure with just negligible nonlinearity in the equatorial regions, but generally stronger nonlinear behavior in the mid-latitudes of both hemispheres. A detailed analysis of the factors behind the observed patterns might be problematic, because they do not seem to be a result of a single driving force, but rather their complex combination. There are, however, some possible links worth mentioning. In the case of the results based on the RT850-500 prediction, there may be a connection between more pronounced nonlinearity in the mid-latitudes and the activity of the polar front. The strongest nonlinear behavior over Europe and North America seems to coincide with the position of the zones where air masses of different origin often interact. In the southern hemisphere, where the landmasses are less extensive, areas of the strongest nonlinearity are typically located rather east of the continents, possibly because of the interaction of the landmass with the prevailing westerlies. Between approximately 50°S and 60°S , where the amount of land is very small, nonlinearity is weaker on average. A removal of the annual cycle from the series slightly decreases the magnitude of detected nonlinearity, but except for the regions where the annual variation is very strong (East Asia), the effect of the annual cycle presence does not dominate the results. For the H850 forecast, there appears to be a certain connection of the areas with strong nonlinearity to the zones of high horizontal gradient of H850. In the northern hemisphere, such areas are typically associated with deep stationary cyclones, which are usually present over the North Atlantic and North Pacific during winter. The match is not perfect though, and there may be some other factors involved. Altogether, it seems that nonlinearity tends to be stronger in the regions with more complex dynamics, where strong driving or perturbing factors are in effect. This hypothesis is supported by the fact that nonlinearity is generally more pronounced during the colder season in the mid-latitudes of both hemispheres, i.e., in situations when the temperature gradient between the equatorial area and the polar region is strongest. The fact that the seasonal variations are more distinct in the northern hemisphere is probably an effect of the uneven distribution of the continents, resulting in a larger influence of the continental climate in the northern mid-latitudes.

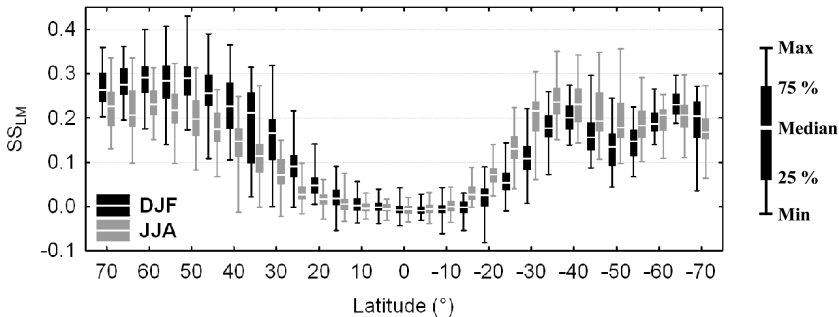


Fig. 10: Distribution of SS_{LM} , obtained for the prediction of RT850-500 for the DJF and JJA seasons in different latitudes (NCEP/NCAR data).

Table 3: Seasonal variations of nonlinearity (expressed by SS_{LM}) in the NCEP/NCAR and HadCM3 data, for the RT850-500 prediction.

Area	NCEP/NCAR		HadCM3	
	DJF	JJA	DJF	JJA
25°N–70°N	0.23	0.16	0.27	0.20
20°S–20°N	0.01	0.01	0.02	0.02
70°S–25°S	0.16	0.20	0.16	0.18

The two presented cases, based on the prediction of geopotential height and relative topography one day ahead, represent just a fraction of possible settings. From additional tests, carried out for different predictand-predictors combinations, it seems that the basic structure with weak nonlinearity in the equatorial area is typical for most situations. On the other hand, the finer details of the detected patterns vary, especially with the type of the predictand. The exact number and geographical configuration of predictors seem to be less important, as long as they sufficiently characterize the local state of the atmosphere. Beside the type of the studied variables, we also paid attention to the sensitivity of the results to the specific details of the tests. It appears that the results are rather robust to the changes of the size of the source area of predictors, although a use of a too big or too small area leads to a general increase of the prediction error and a weakening of detected nonlinearity. The outcomes remain very similar when the input data are pre-processed by principal component analysis, instead of using the point-wise predictors directly. The method of eventual normalization of the predictors also does not appear to be of major importance. The observed patterns of nonlinearity seem to be rather stable in time, i.e., the specific choice of the analyzed period does not have any major effect on the outcomes of the tests. The relatively most distinct changes compared to the presented results were detected in the

NCEP/NCAR data when the 1960s were chosen as the testing set instead of the years 1991–2000, especially in the southern hemisphere. This difference can probably be contributed to the variations in the amount of observational data, entering the reanalysis, as discussed below. The applied tests were all based on prediction one day ahead – with an increase of the lead time, nonlinearity quickly weakened and it became undetectable for predictions more than approximately five days ahead, even in the regions where the nonlinear behavior was originally strongest. This is in good agreement with the fact that a deterministic weather prediction is impossible for too long lead times, regardless of the method.

Most of the patterns of nonlinearity identified in the NCEP/NCAR reanalysis data were also found in the outputs of the HadCM3 model. From the perspective of applied nonlinear time series analysis tasks (such as statistical downscaling carried out by nonlinear methods), the fact that a climate model is able to reproduce the character of the observed data is encouraging. Still, from the results obtained for a single representative of global climate models, it is not possible to infer whether all existing climate simulations do behave in a similar fashion. It is interesting that the correspondence of the structures found in the NCEP/NCAR and HadCM3 data tends to be better in the northern hemisphere. Although this fact can at least partially be a consequence of the specifics of the model's physics, it might also be contributed to the character of the reanalysis data. To assess the possible influence of the specific properties of the NCEP/NCAR reanalysis, we repeated some of the tests for another commonly used gridded dataset based on observations, the ERA-40 reanalysis [28]. Although some differences were found, the resemblance of the results from the NCEP/NCAR and ERA-40 data was generally strong in the northern hemisphere, but somewhat weaker in the southern one. This implies that caution is needed in interpretation of the model-reanalysis differences, particularly in the southern latitudes, as they may be a result of a limited amount of observational data used by the reanalysis (and possibly some other specifics of the NCEP/NCAR dataset), not just imperfections of the climate model. This especially applies to the period preceding the era of meteorological satellites – e.g., the amount of data entering the NCEP/NCAR reanalysis is very low before the year 1979 south of approximately 40°S [19].

We have shown that the direct comparison of prediction by linear regression and by local linear models yields nonlinearity patterns very similar to the approach based on the application of local linear models for surrogate data. A practical advantage of the direct comparison lies in its speed, as there is no need for multiple realizations of a nonlinear model. This is especially convenient in the case of an analysis like ours, carried out for thousands of grid points and repeated for numerous settings. Another benefit of the direct comparison is that it provides specific information about the potential gain from employing a nonlinear method; its fundamental drawback is that such information may only be valid for the combination of the methods applied.

7 Conclusions

By analyzing the series of selected atmospheric variables, we were able to confirm the presence of systematic geographical and seasonal variations of nonlinearity. Simple and unequivocal physical explanation of the results beyond the basic tropics/mid-latitudes and summer/winter contrast may be problematic, because the finer details of the detected patterns are probably a product of multiple influences and they are subject to the type of the predictand variable and some other factors. To find out whether any other general regularities exist would require a systematic analysis performed for a large number of variables and pressure levels. Regardless of the exact cause of the detected structures, their character was simulated fairly well by the HadCM3 model. From the practical perspective, this finding is rather promising, as it confirms that data produced by the current generation of global climate models can be utilized for the study of nonlinear properties of the climate system.

Acknowledgements. This study was supported by the Czech Science Foundation (grant 205/06/P181) and by the Ministry of Education of the Czech Republic (research plan MSM0021620860). The presented work would not be possible without the utilized datasets: NCEP/NCAR reanalysis (obtained from NOAA/OAR/ESRL PSD, Boulder, Colorado, USA, from their Web site at <http://www.cdc.noaa.gov>), HadCM3 model outputs (provided by the Met Office Hadley Centre) and ERA-40 reanalysis (obtained from the Data Server of the European Centre for Medium-Range Weather Forecasts). The authors would also like to express their gratitude to the two anonymous reviewers of the manuscript and to R. Donner for their valuable comments and suggestions.

References

1. M. Paluš, D. Novotná: Testing for nonlinearity in weather records, *Phys. Lett. A* **193**, 67 (1994)
2. D. A. S. Patil, B. R. Hunt, J. A. Carton: Identifying low-dimensional nonlinear behavior in atmospheric data, *Mon. Weather Rev.* **129**, 2116 (2001)
3. J. Miksovsky, A. Raidl: Testing for nonlinearity in European climatic time series by the method of surrogate data, *Theor. Appl. Climatol.* **83**, 21 (2006)
4. M. C. Casdagli: Characterizing Nonlinearity in Weather and Epilepsy Data: A Personal View. In: *Nonlinear Dynamics and Time Series*, ed by C. D. Cutler, D. T. Kaplan (American Mathematical Society, Providence, Rhode Island 1997) pp 201–222
5. G. Sugihara, M. Casdagli, E. Habjan, et al.: Residual delay maps unveil global patterns of atmospheric nonlinearity and produce improved local forecasts, *P. Natl. Acad. Sci. USA* **96**, 14210 (1999)
6. J. Miksovsky, A. Raidl: Testing the performance of three nonlinear methods of time series analysis for prediction and downscaling of European daily temperatures, *Nonlinear Proc. Geoph.* **12**, 979 (2005)
7. M. Paluš: Detecting nonlinearity in multivariate time series, *Phys. Lett. A* **213**, 138 (1996)

8. A. A. Tsonis: Probing the linearity and nonlinearity in the transitions of the atmospheric circulation, *Nonlinear Proc. Geoph.* **8**, 341 (2001)
9. T. Schreiber, A. Schmitz: Surrogate time series, *Physica D* **142**, 346 (2000)
10. I. Bartos, I. M. Jánosi: Nonlinear correlations of daily temperature records over land, *Nonlinear Proc. Geoph.* **13**, 571 (2006)
11. V. Pérez-Muñuzuri, I. R. Gelpi: Application of nonlinear forecasting techniques for meteorological modeling, *Ann. Geophysicae* **18**, 1349 (2000)
12. B. Tang, W. W. Hsieh, A. H. Monahan, F. T. Tangang: Skill comparisons between neural networks and canonical correlation analysis in predicting the equatorial Pacific sea surface temperatures, *J. Climate* **13**, 287 (2000)
13. A. Weichert, G. Bürger: Linear versus nonlinear techniques in downscaling, *Climate Res.* **10**, 83 (1998)
14. J. T. Schoof, S. C. Pryor: Downscaling temperature and precipitation: A comparison of regression-based methods and artificial neural networks, *Int. J. Climatol.* **21**, 773 (2001)
15. M. Casaioli, R. Mantovani, F. P. Scorzoni, et al.: Linear and nonlinear post-processing of numerically forecasted surface temperature, *Nonlinear Proc. Geoph.* **10**, 373 (2003)
16. E. Eccel, L. Ghielmi, P. Granitto, et al.: Prediction of minimum temperatures in an alpine region by linear and non-linear post-processing of meteorological models, *Nonlinear Proc. Geoph.* **14**, 211 (2007)
17. W. von Bloh, M. C. Romano, M. Thiel: Long-term predictability of mean daily temperature data, *Nonlinear Proc. Geoph.* **12**, 471 (2005)
18. E. Kalnay, M. Kanamitsu, R. Kistler, et al.: The NCEP/NCAR 40-year reanalysis project, *Bull. Amer. Meteor. Soc.* **77**, 437 (1996)
19. R. Kistler, E. Kalnay, W. Collins, et al.: The NCEP-NCAR 50-year reanalysis: Monthly means CD-ROM and documentation, *Bull. Amer. Meteor. Soc.* **82**, 247 (2001)
20. C. Gordon, C. Cooper, C. A. Senior, et al.: The simulation of SST, sea ice extents and ocean heat transports in a version of the Hadley Centre coupled model without flux adjustments, *Clim. Dynam.* **16**, 147 (2000)
21. T. C. Johns, J. M. Gregory, W. J. Ingram, et al.: Anthropogenic climate change for 1860 to 2100 simulated with the HadCM3 model under updated emissions scenarios, *Clim. Dynam.* **20**, 583 (2003)
22. E. Ott, T. Sauer, J. A. Yorke (eds.): *Coping with Chaos: Analysis of Chaotic Data and The Exploitation of Chaotic Systems* (John Wiley & Sons, New York 1994)
23. H. Kantz, T. Schreiber: *Nonlinear Time Series Analysis* (Cambridge University Press, Cambridge 1997)
24. D. S. Wilks: *Statistical Methods in the Atmospheric Sciences*, 2nd edn (Elsevier, Amsterdam 2006)
25. V. Venema, S. Bachner, H.W. Rust, C. Simmer: Statistical characteristics of surrogate data based on geophysical measurements, *Nonlinear Proc. Geoph.* **13**, 449 (2006)
26. T. Schreiber, A. Schmitz: Improved surrogate data for nonlinearity tests, *Phys. Rev. Lett.* **77**, 635 (1996)
27. R. Hegger, H. Kantz, T. Schreiber: Practical implementation of nonlinear time series methods: The TISEAN package, *CHAOS* **9**, 413 (1999)
28. S. M. Uppala, P. W. Kållberg, A. J. Simmons, et al.: The ERA-40 re-analysis, *Quart. J. R. Meteorol. Soc.* **131**, 2961 (2005)

Nonlinear Time Series Analysis in the Geosciences
Applications in Climatology, Geodynamics and
Solar-Terrestrial Physics

Donner, R.V.; Barbosa, S.M. (Eds.)

2008, XIV, 390 p., Hardcover

ISBN: 978-3-540-78937-6